Musculoskeletal Simulation-Based Multi-Criteria Optimization Framework for Exoskeleton Design

Ali KhalilianMotamed Bonab and Volkan Patoglu, *Member, IEEE*

***Abstract*— Robotic exoskeletons can enhance human locomotion by reducing its metabolic cost. Designing effective wearable assistive devices requires a systematic approach that accounts for the influence of device kinematics/dynamics and effects of assistance torques on human performance. While comprehensive human-subject experiments to evaluate multiple designs are often impractical, musculoskeletal simulations can serve as a powerful tool for optimizing exoskeleton designs and their corresponding assistance strategies. This paper presents a *musculoskeletal simulation-based multi-criteria design optimization framework* to systematically evaluate and compare various exoskeleton configurations under realistic physical constraints. In this study, the multi-criteria optimization framework is used to characterize the trade-off between metabolic efficiency and power use of mono- and bi-articular lower-limb exoskeleton configurations under optimal assistance torques. The multi-criteria optimization results provide a fair basis for rigorous comparison among various exoskeleton configurations and their corresponding optimal assistance torque profiles, considering realistic actuator saturation limits and the detrimental effects of exoskeleton reflected inertia on metabolic consumption. The results offer valuable insights to guide assistive exoskeleton designs under real-world constraints.**

***Index Terms*— Musculoskeletal simulations, Pareto optimization, exoskeleton design, metabolic cost reduction, energy efficiency, optimization of assistive torque profiles.**

I. Introduction

HUMAN locomotion is versatile and energy-efficient, but can decline due to aging, disease, or injury, leading to reduced mobility and independence. Wearable assistive devices can enhance musculo-tendon efficiency during locomotion. Exoskeletons may aid rehabilitation and/or mitigate injury risks associated with repetitive tasks, such as walking with a load.

Received 2 May 2025; revised 31 October 2025; accepted 19 January 2026. Date of publication 28 January 2026; date of current version 6 February 2026. This work was supported in part by Sabanci University and The Scientific and Technological Research Council of Turkiye (TUBITAK) under Grant 216M200 and Grant 23AG003. *(Corresponding author: Volkan Patoglu.)*

Ali KhalilianMotamed Bonab is with the Institute of Mechanical Intelligence and the Department of Excellence in Robotics and AI, Scuola Superiore Sant'Anna, 56127 Pisa, Italy.

Volkan Patoglu is with the Faculty of Engineering and Natural Sciences, Sabanci University, 34956 Istanbul, Türkiye (e-mail: vpatoglu@sabanciuniv.edu).

This article has supplementary downloadable material available at https://doi.org/10.1109/TNSRE.2026.3658597, provided by the authors.

Digital Object Identifier 10.1109/TNSRE.2026.3658597

Assistive lower extremity exoskeletons primarily aim to reduce the metabolic cost of locomotion. Although early designs struggled to achieve this, recent studies have demonstrated success. Malcolm et al. [1] first reported a significant metabolic reduction using a tethered ankle exoskeleton. Mooney et al. [2] and Collins et al. [3] later achieved reductions with untethered ankle devices. For running, both hip and ankle exoskeletons [4], [5], [6] were reported to improve metabolic efficiency.

Since these pioneering studies, various exoskeletons have further reduced metabolic cost. Most of these exoskeletons assist the hip or ankle, with the exception of an untethered knee exoskeleton used for incline walking with load [7]. Reported reductions are in the range of 5.4%-17.4% for tethered and 3.3%-19.8% for untethered devices [8]. Hip exoskeletons generally outperform ankle-based designs, achieving up to 19.8% improvement compared to 12% for ankle devices. Running performance has been improved with assistance to both the hip and ankle, with passive exoskeletons reducing metabolic cost by 6.4%-8.0% and active ones by 3.9%–14.6%.

Despite significant progress in exoskeleton design, no systematic mechatronic approach exists for the optimal design of exoskeletons to reduce the metabolic cost of human locomotion. Such an approach would require a rigorous and fair comparison of various exoskeleton designs and their corresponding assistance torque profiles. However, comprehensive human subject experiments to evaluate a wide range of designs are generally impractical. Human-in-the-loop studies are challenging because they necessitate the development of multiple prototypes, extensive volunteer recruitment, stringent safety protocols, and a sufficient number of trials to achieve statistical reliability. In addition, difficulties in acquiring certain data without invasive sensors [9], limitations in measuring some parameters [10], and the effects of training/fatigue on performance [11] further restrict experimental studies.

Musculoskeletal simulation studies can complement human-subject experiments by reducing the need for physical prototyping and allowing for fast, automated, and repeatable evaluations in a controlled environment. These simulations enable systematic analysis of exoskeleton design choices without the risks and logistical constraints of human trials. Recent works have also shown that simulation-derived assistance strategies can lead to effective assistance in experimental setups, validating their use for exoskeleton design and demon-

strating how simulation-informed approaches can translate into real-world use [12], [13], [14]. Musculoskeletal simulation studies have been employed to design, optimize, and analyze various assistive devices [15], [16], yielding assistance profiles that deviate from scaled biomimetic joint moments [9], [17], explaining experimentally observed muscle-level effects [18], [19], and suggesting new strategies for impaired gait cycles [20].

Musculoskeletal simulation efforts can broadly be classified into three groups as quasi-static/kinetostatic simulations [15], [21], dynamic simulations that track a set of desired kinematics [9], [17], [22], [23], and predictive simulations [24], [25], [26]. Quasi-static simulations are useful for studying the effects of geometry and load distribution when motion is not involved. Most musculoskeletal studies utilize dynamic simulations that track human kinematics from motion capture data, as this approach can effectively model high-fidelity musculoskeletal dynamics and muscle recruitment while simulating the captured movement, as long as the model dynamics are kept compatible with the conditions of the data capture. Finally, predictive simulations use optimal-control formulations to predict the resulting movement under the musculoskeletal dynamics.

As motion is involved, quasi-static simulations are not appropriate for the determination of assistance torques during walking. While predictive simulations can be powerful, the computational complexity of the underlying optimal control problem severely limits the feasibility of employing musculoskeletal models with many muscles [25]. Along these lines, dynamic simulations that track kinematics from human motion captures have predominantly been employed to study actuator morphologies for exoskeletons under optimal assistance torques [9], [17], [22], [23]. These studies investigate how actuator placement influences performance, typically assuming *idealized* (massless and limitless) actuators. On the other hand, considering the metabolic cost of inertial effects and computing assistance torque profiles under actuator-specific joint torque constraints are crucial for real-life applicability.

Previous studies do not address the inherent device-level trade-offs between metabolic cost reduction and device power consumption. Neither do they consider realistic inertial effects and joint-specific torque limits. In practice, high metabolic reductions require large torque outputs, resulting in high power consumption, whereas energy-efficient, lightweight designs rely on compact actuators that can provide lower torques. Accordingly, there is a need for addressing a *multi-criteria design optimization problem* that jointly considers metabolic benefit and actuator power, handles joint-specific torque limits, and accounts for device mass and reflected inertia.

In this study, we introduce a multi-criteria design framework that systematically evaluates and compares exoskeletons under realistic constraints by *co-optimizing* metabolic benefit and device power metrics via musculoskeletal simulations. Unlike prior studies that rely on idealized actuators, it enforces joint-specific torque limits and considers device power over the gait cycle while computing the optimal assistance torques. In addition, it also incorporates the mass and reflected inertia of the actuators to yield a realistic set of non-dominated solutions that balance metabolic cost reduction and power consumption. To demonstrate the proposed approach, we compare bi-articular and mono-articular exoskeleton configurations under no-load and loaded walking conditions. We independently vary hip and knee torque limits to compute the optimal assistance torques, and then superpose an empirically determined metabolic cost of reflected actuator inertia onto the set of non-dominated solutions. The results constitute a set of optimal solutions that provide a fair basis for rigorous comparison among various exoskeleton designs. Overall, the proposed musculoskeletal simulation-based multi-criteria optimization framework provides *guidelines* for the design of effective assistive exoskeletons under realistic constraints.

II. Musculoskeletal Simulations

Musculoskeletal simulations were conducted using OpenSim, an open-source platform widely used in movement science [10], [27]. Although musculoskeletal modeling has inherent limitations [28], OpenSim provides robust biomechanical models and simulation tools that have been effectively used to design and evaluate assistive devices [9], [17], [23], [29], [30], [31].

In this study, two powered exoskeleton configurations were evaluated by simulating seven subjects walking under two conditions: *noload* (walking at self-selected speeds without additional weight) and *loaded* (walking while carrying a 38 kg torso load). The simulations employ a three-dimensional musculoskeletal model developed by Rajagopal et al. [32], which features 37 degrees of freedom. The lower limbs are actuated by 80 massless musculotendon actuators, and the upper limbs by 17 torque actuators. For the purposes of our analysis, degrees of freedom deemed non-essential–namely, ankle eversion, toe flexion, wrist flexion, and wrist deviation–were locked. The additional torso load in the loaded condition was modeled following the approach detailed in [17].

A. Experimental Data

Similar to previous studies [30], [33], our simulations were based on experimental data collected from seven male subjects, as reported by Dembia et al. [17]. The dataset includes both motion capture and ground reaction force measurements recorded under natural and 38 kg weight-bearing conditions.

B. Modeling of Assistive Devices

We consider two powered exoskeleton configurations (mono-articular and bi-articular) for active assistance of the bilateral hip and knee joints. The bi-articular design, inspired by the arrangement of bi-articular muscles, concentrates much of the device's mass at the proximal hip while delivering power to the distal knee. This configuration leverages bi-articulation, which has been shown to enhance bipedal locomotion efficiency [34]. In contrast, the mono-articular exoskeleton directly assists each joint through actuators mounted at the respective joints.

To facilitate power transmission in the bi-articular device, a parallelogram mechanism is utilized. This mechanism enables

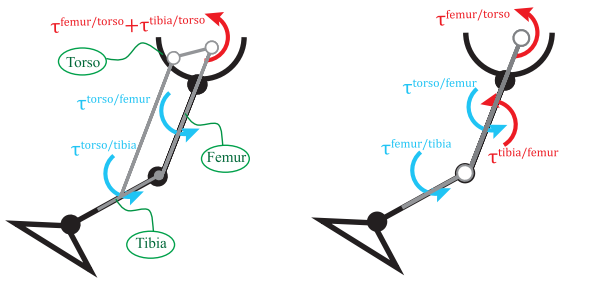

(a) bi-articular exo (b) mono-articular exo

Fig. 1. Actuator model of assistive devices. Blue and red arrows indicate the action and reaction torques, respectively. Exoskeleton links corresponding to the tibia and femur are rigidly attached to the leg segments, while both exoskeletons are attached to the torso.

effective power transfer from the hip to the knee, promotes regeneration between adjacent joints [35], [36], facilitates joint coupling [34], and improves the distribution of muscle load and leg inertia [34]. In contrast, the mono-articular exoskeleton is modeled as a two-link serial manipulator with actuators directly attached to the assisted joints. Kinematic models of exoskeletons are provided in *Supplementary Material* S1.

The relationship between the kinematics of monoarticular and biarticular exoskeletons can be established through linear mapping J as expressed in Eqn. (1)

$$\omega_{\text{mono}} = J \ \omega_{\text{bi}}$$
$$\begin{bmatrix} {}^{\text{torso}}\omega_{\text{mono}}{}^{\text{femur}} \\ {}^{\text{femur}}\omega_{\text{mono}}{}^{\text{tibia}} \end{bmatrix} = \begin{bmatrix} 1 & 0 \\ -1 & 1 \end{bmatrix} \begin{bmatrix} {}^{\text{torso}}\omega_{\text{bi}}{}^{\text{femur}} \\ {}^{\text{torso}}\omega_{\text{bi}}{}^{\text{tibia}} \end{bmatrix} \quad (1)$$

where ${}^{\text{torso}}\omega_{\text{mono}}^{\text{femur}}$ and ${}^{\text{femur}}\omega_{\text{mono}}^{\text{tibia}}$ denote the angular velocities of the mono-articular actuators, while ${}^{\text{torso}}\omega_{\text{bi}}^{\text{femur}}$ and ${}^{\text{torso}}\omega_{\text{bi}}^{\text{tibia}}$ represent those of the bi-articular configuration.

To model an ideal exoskeleton in the OpenSim framework, TorqueActuator class provided by OpenSim API is utilized. This type of actuator applies equal and opposite torques to the two bodies it connects. Along these lines, the action and reaction torques of the bi-articular and mono-articular exoskeletons are assigned, as shown in Fig. 1. As presented in Fig. 1(a), both torque actuators of the bi-articular exoskeleton are located at the torso; hence, the reaction forces of these actuators are applied to the torso, which matches the kinematics and dynamics model of the bi-articular exoskeleton

$$\tau_{bi}^{hip} = \tau^{torso/femur} \qquad \tau_{bi}^{knee} = \tau^{torso/tibia}$$

where $\tau_{\text{bi}}^{\text{torso/femur}}$ and $\tau_{\text{bi}}^{\text{torso/tibia}}$ stand for torques of the bi-articular hip and knee actuators, respectively.

The mono-articular exoskeleton depicted in Fig. 1(b) is modeled by assigning the action torque of the hip joint actuator from the torso to the femur and the action torque of the knee joint actuator from the femur to the tibia

$$\tau_{mono}^{hip} = \tau^{torso/femur} \qquad \tau_{mono}^{knee} = \tau^{femur/tibia}$$

where $\tau_{\text{mono}}^{\text{torso/femur}}$ and $\tau_{\text{mono}}^{\text{femur/tibia}}$ represent the torques of the mono-articular hip and knee actuators, respectively.

The transpose of the linear map J in Eqn. (1) provides the mapping between the torques provided by exoskeletons as

$$\tau_{\text{bi-articular}} = J^T \ \tau_{\text{mono-articular}} \quad (2)$$

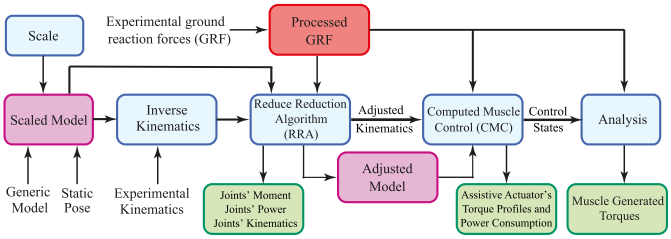

Fig. 2. Block diagram of OpenSim simulation. Green blocks represent outputs, blue blocks represent OpenSim simulations or analyses, purple blocks represent models used for simulations and analyses, and red blocks represent experimentally captured data.

where $\tau_{\text{bi-articular}}$ and $\tau_{\text{mono-articular}}$ represent the torques of the bi- and mono-articular exoskeletons, respectively. If no saturation limits exist on the actuator velocities or torques, then the linear mapping J^T between the exoskeletons dictates that they can provide the same level of assistance with the same amount of power consumption under ideal conditions. It is important to note that the linear mapping between the mono- and the bi-articular exoskeletons no longer holds if the hip and knee actuators have velocity or torque saturation, as considered in this study.

C. Musculoskeletal Simulation Workflow

Fig. 2 summarizes our OpenSim simulation workflow. First, the generic dynamic model is scaled using the OpenSim Scale Tool to match each subject's anthropometry, with muscle maximum isometric forces adjusted according to mass and height. Next, the OpenSim Inverse Kinematics Tool maps experimental motion capture data to joint angle trajectories.

In the second step, any discrepancies between the experimental data (ground reaction forces and motion capture) and the scaled model are minimized by adjusting the model's inertial properties and kinematics through OpenSim's Residual Reduction Algorithm (RRA) [27].

In the third step of our simulation workflow, we employ the Computed Muscle Control (CMC) algorithm [37] to determine muscle activations that best replicate the experimentally captured kinematics. The CMC algorithm resolves muscle redundancy by solving a least-squares optimization problem. In its standard formulation, the objective function is

$$J = \sum_{i \in nMuscles} a_i^2 + \sum_{i \in nReserves} \left(\frac{\tau_{r,i}}{w_{r,i}} \right)^2 \quad (3)$$

where a_i^2 is the activation level of a muscle i, $\tau_{r,i}$ is the torque produced by the i^{th} reserve actuator, and $w_{r,i}$ are the weights of the reserve actuators. In OpenSim, the reserve actuators are included to account for model uncertainties and unmodeled dynamics, and their weights are set to low values to strongly penalize their use.

In order to include the effects of assistive devices in musculoskeletal simulations, assistive torques provided by the actuators of the exoskeleton need to be considered as part of the CMC algorithm. Along these lines, assistive torques provided by OpenSim Torque Actuators need to be added to the objective function of the CMC algorithm. Accordingly,

the objective function is adjusted as in Eqn. (4) to enable the inclusion of assistive torques.

$$J = \sum_{i \in nMuscles} a_i^2 + \sum_{i \in nExo} \left(\frac{\tau_{exo,i}}{w_{exo,i}} \right)^2 + \sum_{i \in nReserves} \left(\frac{\tau_{r,i}}{w_{r,i}} \right)^2 \quad (4)$$

where $\tau_{exo,i}$ is the torque provided by actuator i and $w_{exo,i}$ represents the weights of the exoskeleton actuators, which are used to penalize the utilization of the torque actuators. By setting $w_{exo,i}$ to a high value (selected as 1000 Nm in our study), the penalty for utilizing exoskeleton assistance is reduced, thereby encouraging the optimizer to make greater use of assistive torques during the gait cycle.

Muscle activations and exoskeleton torques obtained from this modified CMC algorithm serve as the basis for calculating key biomechanical outputs, such as metabolic power consumption, muscle moments, and joint reaction forces, using the OpenSim Analysis Tool.

D. Metabolic Model

To estimate instantaneous metabolic power, we employ Umberger's muscle energetic model [38] as modified by Uchida et al. [39]. The average power consumption of a muscle over a gait cycle is calculated as

$$P_{avg} = \frac{m_{muscle}}{t_f - t_0} \int_{t_0}^{t_f} P(t), dt, \quad (5)$$

where m_{muscle} denotes muscle mass, $P(t)$ is the normalized metabolic power at time t, and t_0 and t_f are the initial and final times of the gait cycle. The overall metabolic power is obtained by summing the contributions of all muscles and then normalizing the integrated value over the gait cycle by the subject's mass. For the assisted conditions, the same model is used to compute instantaneous metabolic power. Its integration over the gait cycle yields the subject's metabolic rate.

III. Multi-Criteria Optimization and Comparison

During musculoskeletal simulations in OpenSim, the CMC algorithm resolves muscle redundancy by minimizing a weighted sum-of-squares objective function at each time step [28]. In studies of *ideal* exoskeletons, assistance torques are maximized by assigning high assistance torques to the exoskeleton actuators, effectively ignoring the physical constraints of real devices. However, practical exoskeleton designs must navigate substantial trade-offs among power consumption, metabolic cost reduction, and dynamic properties.

Because metabolic cost reduction and device power consumption are inherently conflicting objectives, no single design can optimize both simultaneously. Moreover, the trade-off between these metrics is not immediately apparent, making the assignment of relative importance non-trivial. Consequently, a multi-criteria design optimization problem needs to be solved to capture their inherent trade-off.

While scalarization methods can combine these objectives into a single aggregate cost function using predetermined weights, such approaches force designers to assign pReferences a priori, before the trade-off landscape is known. Therefore, we advocate for a Pareto optimization approach in musculoskeletal simulation-based design. Rather than computing a unique solution, Pareto optimization seeks to generate a set of mathematically equivalent, non-dominated solutions, each representing a design where an improvement in one objective necessitates a degradation in the other. The collection of these solutions forms the Pareto-front [40], [41], [42]. The Pareto-front allows designers to examine optimal designs corresponding to different preferences and to introduce other (primary and secondary) design criteria during the design selection stage.

Moreover, by imposing realistic constraints on the actuator torques, our Pareto method produces optimal solutions for each exoskeleton configuration with the corresponding optimal assistance torque profiles, *capturing the optimal performance across all design preferences*, as depicted in Fig. 3. This approach enables fair and systematic comparisons among devices with different underlying kinematics, dynamics, actuation, or even under different loading conditions [43], [44], [45].

The Pareto approach is implemented in three stages: (i) Selection and evaluation of performance metrics, (ii) computation of the Pareto-front solutions, and (iii) selection of an optimal solution from the non-dominated set.

A. Performance Metrics

The objective is to design an energy-efficient untethered wearable exoskeleton that reduces metabolic cost. Following the hierarchical classification in [46], design requirements are categorized as imperative, optimal, primary, and secondary.

Ensuring the safety of physical human-robot interaction and an ergonomic fit are imperative design requirements for exoskeleton-type wearable assistive devices. The safety of physical human-robot interaction can be ensured by guaranteeing coupled stability of low-level interaction controllers [47], [48], [49], [50], [51], [52], while ergonomic fit can be achieved through the implementation of proper joint alignment mechanisms [53], [54], [55], [56], [57]. Both of these objectives must be considered during the physical implementation of the mechatronic system; hence, they lie beyond the scope of this design study.

In this study, we focus on two optimal performance metrics: metabolic cost reduction and energy efficiency. In our simulations, the normalized whole-body metabolic rate for each subject, estimated under both assisted and unassisted conditions (with and without a 38 kg load), is used to compute the percentage reduction in metabolic cost. Simultaneously, energy efficiency is quantified by computing the absolute power consumption of the exoskeleton actuators, defined as the integral of the absolute instantaneous actuator power over the gait cycle. It should be noted that the actuator power consumption metric also indirectly reflects device weight and inertia since more power-efficient devices can be implemented with lighter components. These optimal metrics are maximized *simultaneously*, yielding *non-dominated solutions* for each exoskeleton configuration.

Dynamic simulations based on tracking pre-recorded kinematics require the model dynamics to be kept compatible

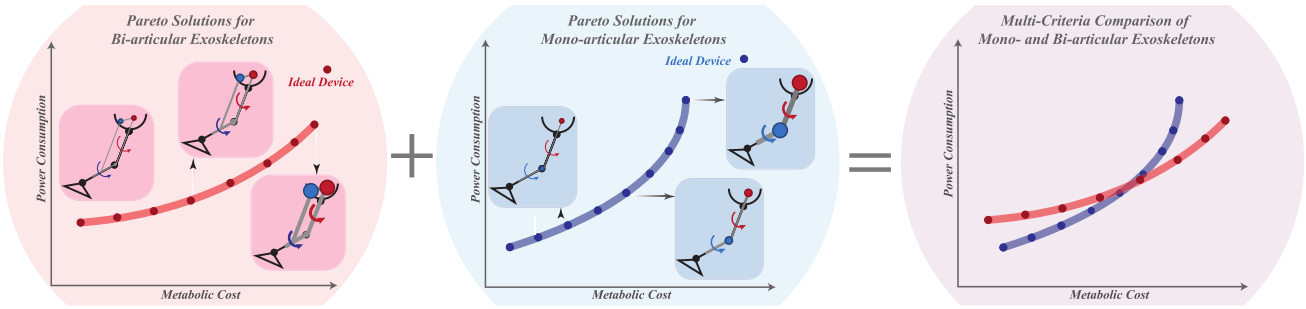

Fig. 3. Schematic representation of a multi-criteria comparison of bi-articular and mono-articular exoskeletons. The blue and red curves denote the Pareto-fronts for mono- and bi-articular devices, respectively. Each point on the Pareto-front represents a non-dominated solution—an optimal design tailored to a specific designer preference. The Pareto-optimal set includes the "ideal" devices at the limits, which maximize metabolic cost reduction by ignoring power consumption. By analyzing these non-dominated solutions, a rigorous and fair comparison of different exoskeleton configurations is achieved, capturing the best possible performance for all design preferences.

with the conditions of the data capture; hence, the inertia of the actuators cannot be directly included in such simulations. Since primary design requirements are considered after the multi-criteria optimization problem is solved with respect to the optimal performance metrics, the inertial effects are considered through a primary design requirement, mandating the device be lightweight with low reflected inertia. In particular, once non-dominated solutions are computed, an empirically determined model [58] of metabolic burden of added mass/inertia on the human body segments is superposed on these results to yield inertia-adjusted Pareto solutions. The separation of musculoskeletal simulation from the inertial influences is not only a necessary step for the validity of dynamic simulations based on tracking pre-recorded kinematics, but also a useful approach for design, as it allows Pareto solutions to be used in a multi-shot manner, enabling flexible integration of different actuator types into the design framework.

We consider the cost of carrying (CoC) [17] as another primary design metric. To evaluate CoC, we compute the average and standard deviation of the maximum positive power of actuators of each exoskeleton configuration. Additional primary requirements considered include changes in the muscle activities of key lower-limb muscles and variations in joint reaction forces and moments under assistance. These factors are evaluated for inertia-adjusted Pareto solutions to further guide the design selection.

Finally, the secondary requirements for the exoskeleton may be considered as ease of implementation, robustness, and device cost. The secondary requirements are imposed by the designer based on the specific use scenario; hence, these considerations are outside the scope of this study.

B. Computation of the Pareto-Front Solutions

The most commonly used Pareto optimization approaches include frontier-construction methods [59], [60], [61]. In this study, we perform simultaneous maximization of metabolic cost reduction (f_1) and minimization of device power consumption (f_2). The bi-objective problem is defined as

$$\begin{aligned} &\text{maximize } f_1(\mathbf{x}) : \text{metabolic cost reduction} \\ &\text{minimize } f_2(\mathbf{x}) : \text{device power consumption} \\ &\text{subject to } \mathbf{x} \in X \end{aligned} \tag{6}$$

where $\mathbf{x}$ represents the design variables of the assistance torque trajectories for the knee and hip actuators throughout the gait cycle, while X captures the feasible solutions dictated by human biomechanics and the assistive device, captured by constraints imposed by motion capture and GRF data collected from the users, the kinematics of the underlying exoskeleton configuration, the three-dimensional musculoskeletal model of the lower limb [32], and the actuator torque saturation limits on the knee and hip actuators.

To solve the multi-criteria optimization problem, we prefer the ϵ-constraint method [62], [63], [64], as it is well-suited for use with musculoskeletal simulations and capable of capturing both convex and non-convex regions of the Pareto front. This method transforms the multi-objective problem into a series of single-objective problems by retaining one objective (here, f_1) and converting the other into an inequality constraint with varying bounds as in Eqn. (7).

$$\begin{aligned} &\text{maximize } f_1(\mathbf{x}) \\ &\text{subject to } f_2(\mathbf{x}) \leq \epsilon \quad \text{and} \quad \mathbf{x} \in X. \end{aligned} \tag{7}$$

Systematically varying the constraint bound ϵ, one can explore the trade-off space and obtain the complete set of Pareto-optimal solutions. To ensure strict Pareto optimality and avoid weakly dominated solutions, the results are filtered according to the non-dominance condition.

To implement the ϵ-constraint method within our OpenSim framework, we systematically constrain the peak torque of the assistive actuators. Limiting the maximum assistance torque during a gait cycle directly influences the redundancy resolution of the CMC algorithm, thereby affecting both muscle recruitment and the resulting metabolic cost reduction (see Fig. 5 for this saturation effect). Furthermore, because the subject kinematics do not change in our simulations, actuator saturation provides a systematic upper bound on the device power consumption metric. By varying the maximum allowable torque over a discrete range, we generate a set of optimal solutions in the objective space.

In our study, a symmetry constraint is imposed between the left and right leg actuators. The maximum torques available to the hip and knee actuators are varied from 30 Nm to 70 Nm with 10 Nm increments for both bi-articular and mono-articular exoskeletons. This torque range is representative of many untethered exoskeleton designs [65], [66], [67], [68],

TABLE I
INERTIAL PROPERTIES AND METABOLIC MODEL PARAMETERS OF THE BI-ARTICULAR AND MONO-ARTICULAR EXOSKELETONS

Configuration	Waist		Thigh			Shank			Actuator
	mass (kg)	α	mass (kg)	CoM (m)	α, β, γ	mass (kg)	CoM (m)	α, β, γ	inertia ($kg.m^2$)
bi-articular	4.5	0.045	1	0.23	0.075, -0.74, 1.81	0.9	0.18 + l_{thigh}	0.076, 0.637, 0.409	5.06×10^{-4}
mono-articular	3	0.045	2.5	0.30	0.075, -0.74, 1.81	0.9	0.18 + l_{thigh}	0.076, 0.637, 0.409	5.06×10^{-4}

including our own. While an identical range is used for both joints, torque assignments are varied independently to avoid any a priori joint-specific assumptions and to let the optimization reveal the appropriate actuator allocations.

C. Multi-Criteria Comparison and Design Selection

Once the Pareto-front solutions are computed for each exoskeleton configuration under different loading conditions (see Fig. 3), these solutions can be compared and *an* optimal design can be selected. To facilitate this selection, the primary design requirements, as detailed in Section III-A, are considered.

Since dynamic simulations based on OpenSim/CMC tracks pre-recorded kinematics and can only simulate conditions that are compatible with the data capture, they cannot model inertial effects of an exoskeleton not worn during the capture. Accordingly, after computing the Pareto solutions, we primarily concentrate on including the detrimental effects of added segment mass and reflected inertia. To this end, we compute the metabolic burden of added mass/inertia on the human body segments through the empirical model of Browning et al. [58] and incorporate inertial penalties to the set of non-dominated designs to form *inertia-adjusted* Pareto solutions.

In this context, mass and inertia penalties quantify the metabolic cost of carrying additional weight on a human body segment and the cost associated with resisting acceleration due to the reflected inertia of the exoskeleton about a joint, respectively. These effects are modeled using segment-wise coefficients in [58] and summed to yield the adjusted metabolic rate. In our simulations, the reflected inertia of each actuator is parameterized via the transmission ratio required to meet the specified peak torque capacity. The inertial properties of segments (CoM locations and baseline inertias) follow standard anthropometric definitions [69], as listed in Table I.

For each candidate design, the actuator placement determines the added segment masses. A constant peak torque of 2 Nm is assumed for the actuators, and the transmission ratio N is determined to satisfy a given peak joint torque. Accordingly, the actuator's reflected inertia as seen from the joint is amplified with N^2 and is added to the inertia of the other transmission elements. Segment (thigh and shank) inertias are computed about the hip and updated considering the parallel-axis terms due to added mass. Since actuator placement differs between the mono- and bi-articular exoskeleton configurations, the resulting mass and inertia distributions also differ significantly across configurations, even when the underlying actuator modules are identical. Device-specific numerical values used for the computation of the inertia-adjusted Pareto solutions are reported in Table I.

The segment-wise metabolic rate penalties due to inertial effects are computed according to Eqns. (8)–(9), derived from the Browning's metabolic model [58]

$$\Delta MC_{s,m} = \alpha_s \, m_s \tag{8}$$

$$\Delta MC_{s,I} = (\beta_s + \gamma_s \, I_{s,\text{ratio}}) \, MC_{\text{unassisted}} - MC_{\text{unassisted}} \tag{9}$$

where $\Delta MC_{s,m}$ [W/kg] denotes the change in metabolic cost for the segment s due to the added mass m_s [kg], and α_s is a segment-specific constant. Similarly, Eqn. (9), $\Delta MC_{s,I}$ [W/kg] represents the change in metabolic cost due to the added inertia. $MC_{\text{unassisted}}$ is the baseline metabolic cost of the unassisted condition and $I_{s,\text{ratio}}$ is the ratio of the inertia of the segment with the exoskeleton to the nominal inertia of the segment, i.e., $I_{s,\text{ratio}} = (I_{\text{exo},s} + I_{\text{nominal},s})/I_{\text{nominal},s}$. The coefficients β_s and γ_s are empirically determined for each segment s and are presented in Table I, together with α_s. While segment mass is fixed, the inertia ratio depends on the peak torque capacity via the transmission ratio selected to meet that capacity, yielding larger penalties for higher torque values.

For each Pareto solution, the segment-wise mass and inertia penalties are computed and added to the metabolic rate computed using the musculoskeletal simulations. The inertia-adjusted Pareto solutions are computed by filtering the results according to the non-dominance condition. The inertia-adjusted Pareto solutions capture the trade-offs among metabolic benefit, actuator power, and the metabolic penalties of added mass and reflected inertia due to the exoskeleton.

Models and scripts used in the methods sections are available at https://simtk.org/projects/multicriteria. (Please see *Supplementary Material* S10.)

IV. STATISTICAL ANALYSIS

A total of 2142 musculoskeletal simulations were conducted for seven subjects walking at their preferred speed under two different loading conditions, with each condition repeated for three trials. To assess statistically significant effects and enable multiple comparisons, appropriate statistical tests were performed. Prior to analysis, the normality of the data was verified using the Shapiro-Wilk test in SPSS [70]. An N-way repeated measures ANOVA was conducted to examine the effects of loading condition and exoskeleton configuration on key outcome variables. When a significant main effect or interaction was found, one-way repeated-measures ANOVA was used to further investigate pairwise differences. Tukey's post hoc tests were applied for multiple comparisons when necessary. A significance level of 0.05 was used throughout the study. Only statistically significant differences are explicitly marked in tables and figures to ensure clarity in data presentation.

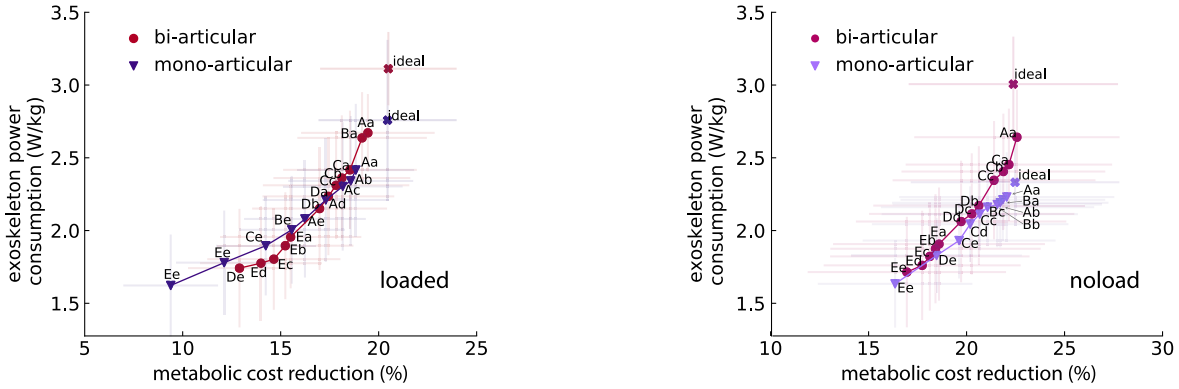

Fig. 4. Pareto-front solutions characterizing the trade-off between metabolic cost reduction and absolute power consumption. The data points on the Pareto-front represent the average and standard deviations over 7 subjects and 3 trials per subject. The label on each marker denotes results from different peak torque constraints. The hip peak torque constraints are labeled with capital letters from *A* to *E* to represent the range of torques from 70 Nm to 30 Nm, while the knee peak torque constraints are labeled with lower-case letters from *a* to *e* to represent the same range.

TABLE II
NORMALIZED AND MAXIMUM POWER CONSUMPTION AND METABOLIC COST REDUCTION OF IDEAL AND TORQUE-LIMITED EXOSKELETONS

Configuration	Device Type	Condition	Hip Power (W/kg)	Knee Power (W/kg)	Metabolic Cost Reduction (%)	Max Hip Power (W)	Max Knee Power (W)
Bi-articular	Ideal	No-load	1.42 ± 0.32	1.58 ± 0.30^{a}	22.38 ± 4.91	4.65 ± 0.75^{f}	5.10 ± 0.81^{g}
	Limited "Db"	No-load	1.03 ± 0.31	1.03 ± 0.14^{a}	20.36 ± 5.39	3.54 ± 0.87^{f}	3.07 ± 0.43^{g}
	Ideal	Loaded	1.58 ± 0.29^{b}	1.52 ± 0.29^{c}	20.49 ± 2.87	4.90 ± 0.76^{h}	5.62 ± 1.55^{i}
	Limited "Db"	Loaded	1.03 ± 0.24^{b}	1.11 ± 0.24^{c}	16.99 ± 3.44	3.06 ± 0.54^{h}	3.26 ± 0.68^{i}
Mono-articular	Ideal	No-load	1.09 ± 0.24	1.24 ± 0.13^{d}	22.47 ± 4.89	2.92 ± 0.44^{j}	4.24 ± 0.74
	Limited "Ce"	No-load	0.98 ± 0.20	1.10 ± 0.15^{d}	20.67 ± 5.01	2.29 ± 0.39^{j}	3.97 ± 0.83
	Ideal	Loaded	1.52 ± 0.28^{e}	1.24 ± 0.27	20.45 ± 2.81	4.08 ± 0.69^{k}	4.24 ± 0.97^{l}
	Limited "Be"	Loaded	1.07 ± 0.17^{e}	0.93 ± 0.22	15.56 ± 2.71	2.67 ± 0.45^{k}	3.19 ± 0.59^{l}

Notes: Superscripts indicate statistically significant differences with $p < 0.05$ between devices (7 subjects, 3 trials).
Average power consumption tests: ^{a} $F(1,12) = 6.284$, $p = 0.028$; ^{b} $F(1,12) = 12.313$, $p = 0.004$; ^{c} $F(1,12) = 4.747$, $p = 0.050$; ^{d} $F(1,12) = 13.591$, $p = 0.003$; ^{e} $F(1,12) = 11.889$, $p = 0.005$
Maximum power consumption tests: ^{f} $F(1,12) = 5.863$, $p = 0.032$; ^{g} $F(1,12) = 39.441$, $p < 0.001$; ^{h} $F(1,12) = 20.082$, $p = 0.001$; ^{i} $F(1,12) = 13.491$, $p = 0.003$; ^{j} $F(1,12) = 8.361$, $p = 0.014$; ^{k} $F(1,12) = 22.015$, $p = 0.001$; ^{l} $F(1,12) = 5.944$, $p = 0.031$

V. RESULTS AND DISCUSSION

A. Multi-Criteria Optimization Results

While studies of ideal exoskeleton optimizations (unbounded by physical limitations) provide many valuable insights, different exoskeleton designs cannot be meaningfully compared without introducing some realistic physical limits on the actuator torques and considering the power consumption of these devices. This subsection introduces different levels of peak torque constraints on the actuators of both mono-articular and bi-articular exoskeleton configurations and compares their performance by *simultaneously* optimizing the metabolic cost reduction and the power consumption metrics.

1) Performance of Optimal (Non-Dominated) Devices: Realistic exoskeletons are inherently constrained by actuator torque and power capabilities, which create trade-offs between assistance level and power consumption. When actuator saturation is introduced, the linear mapping between mono- and bi-articular designs breaks down, leading to distinct assistance torque characteristics. To capture these trade-offs, we employed the ϵ-constraint method within the OpenSim framework, by systematically constraining the peak actuator torque to impose realistic upper bounds on power consumption.

The resulting average Pareto-front solutions for both exoskeleton configurations under *noload* and *loaded* walking conditions are shown in Fig. 4. Pareto-front solutions encompass the "ideal" solutions as a limiting case, where only metabolic cost reduction is optimized. These solutions are annotated as "ideal" and correspond to the solutions with the highest power consumption. This Pareto-front plot captures the non-dominated solutions according to the musculoskeletal simulations and can be used in a multi-shot manner to study the effects of various primary selection criteria, such as inertial penalties, regeneration efficiency, or transmission losses.

One of the most significant findings from the Pareto analysis is that torque-limited exoskeletons with sufficiently high torque capabilities at the hip and knee joints achieve metabolic cost reductions that are statistically indistinguishable from those of ideal exoskeletons, while exhibiting significantly lower power consumption under both *noload* and *loaded* conditions. Table II presents the torque-limited devices on the Pareto-front that achieve the same metabolic cost reduction as the ideal devices; it also confirms that the power consumption and the maximum positive power for these devices are statistically significantly lower under both loading conditions.

The mono-articular and bi-articular exoskeleton configurations, when constrained by torque limits, provide similar levels

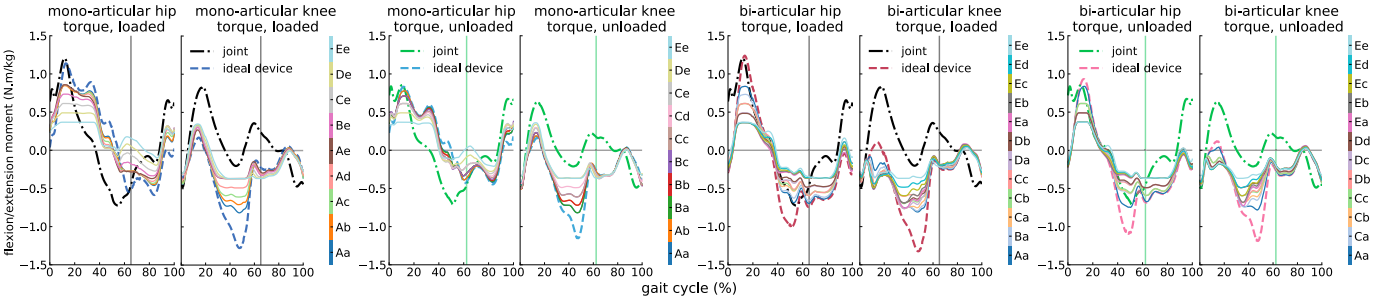

Fig. 5. Torque profiles of the non-dominated exoskeletons together with the joint moments. Each line represents the torque profile of a non-dominated exoskeleton as defined in the color bar.

of assistance—measured by metabolic cost reduction—under both *noload* and *loaded* conditions. However, our Pareto-front analysis reveals that mono-articular devices exhibit slightly lower power consumption under *noload* conditions, though this advantage diminishes under load, where the power consumption becomes nearly identical for both configurations.

For mono-articular exoskeletons, the power distribution analysis (see Fig. C1 of *Supplementary Material* S3) shows that knee actuators are more dominant under *noload* conditions. Under *loaded* conditions, however, the increased mechanical work of the hip actuators makes them the primary contributors (see Fig. C2 of *Supplementary Material* S3). This suggests that for applications involving low loads, designs that focus on knee assistance might enhance energy efficiency and battery life. However, as load increases, the additional work performed by the hip actuators of mono-articular exoskeletons causes overall power consumption to converge with that of bi-articular devices.

In contrast, the power distribution in bi-articular exoskeletons remains largely uniform across loading conditions, with the maximum torque requirements at the hip and knee remaining essentially unchanged. This consistency in performance under different loading conditions implies that bi-articular designs may offer a more robust and predictable assistance strategy, potentially simplifying the control system and reducing the need for adaptive adjustments.

2) Torque Profiles of Non-Dominated Exoskeletons: Fig. 5 presents the assistance torque profiles of non-dominated exoskeleton configurations under torque limits. The profiles serve as reference values for torque controllers, under the assumption that the system has sufficient bandwidth to track them. If control bandwidth limitations are to be considered, then the cost function of the CMC algorithm may be adjusted to include new penalties to impose extra safety-related constraints.

The torque profiles of non-dominated exoskeleton configurations under torque limits deviate from the net joint moments of the hip and knee, though they follow trends similar to those of ideal exoskeletons, as in Fig. 5. The bi-articular hip actuators exhibit notable magnitude differences during the mid-stance and terminal phases. In contrast, the knee actuators of bi-articular exoskeletons closely follow the ideal profiles during the swing, while showing significant differences during the stance phase. Moreover, loading mainly affects the magnitude of the torque-limited profiles without altering their overall trend under both *noload* and *loaded* conditions.

For mono-articular exoskeletons, the hip actuator profiles display considerably greater deviations from the ideal throughout the gait cycle, with saturation occurring from mid-stance to initial swing and pronounced differences taking place during pre-swing to mid-swing phases. Meanwhile, the mono-articular knee actuators exhibit profiles that closely resemble those of the ideal device during the swing, with the primary discrepancies arising during the stance phase. Quantitative comparisons are in Table 1 of *Supplementary Material* S4.

In contrast to the bi-articular configurations, where loading primarily alters the magnitude of the assistance torque without significantly changing its trend, the mono-articular hip actuator profiles vary substantially between *noload* and *loaded* conditions. Under different loads, the hip torque trajectories of mono-articular exoskeletons differ in both shape and magnitude across all gait phases, particularly from load response to mid-swing, making their behavior less predictable.

Some torque-limited bi-articular knee actuators (e.g. bi-articular "Aa" and "Ea" under *noload* condition) exhibit a reversal in assistance torque direction during early stance compared to the ideal profiles. This reversal occurs because, during early stance, the muscle-generated moments exceed the net knee joint moment. In response, the exoskeleton's knee actuators generate an opposing torque that effectively cancels out the excessive muscle moment, thereby keeping the net joint moment on track (see Fig. D1 of *Supplementary Material* S5). Additionally, when the hip actuator saturates, its reduced torque capacity leads to diminished rectus femoris activation and shifts the load to the gastrocnemius, iliopsoas, and vasti muscles. The increased activity of the vasti, combined with excessive rectus femoris output, produces a higher extension moment at the knee during early stance, prompting the knee actuator to adjust its torque direction accordingly.

Similarly, the hip actuators of mono-articular exoskeletons display considerable variability, especially during the pre-swing and initial swing phases (e.g., mono-articular "Ae" and "Ee" under *loaded* condition). Comparisons between different mono-articular configurations under *loaded* conditions indicate that reducing the hip actuator's torque capacity results in decreased rectus femoris activity and increased iliopsoas activation. This altered muscle coordination yields a muscle-generated moment that exceeds the ideal profile during the pre-swing and initial swing, which is then counteracted by

the hip actuator, as in Figs. D3 and D4 of *Supplementary Material* S5.

Notably, the optimization framework favors solutions in which the exoskeleton actuators are highly activated rather than relying on muscles with higher penalization weights. This leads to an optimal solution where the low penalty assigned to the actuators allows them to dominate the redundancy resolution, ensuring that the net joint moment is accurately followed. Such behavior aligns with results by Dembia et al. [17] and Uchida et al. [9], who demonstrated that the optimizer targets a collective activation of the muscle set rather than focusing on individual muscles to achieve a lower overall cost.

Under realistic torque limitations, however, muscle activation patterns can be quite different from those observed with ideal exoskeletons. The constrained actuation forces the neuromuscular system to adapt its coordination strategy, leading to altered muscle recruitment that better reflects the musculoskeletal system's response to assistance. By incorporating realistic saturation limits, our simulations provide a more accurate representation of exoskeleton performance in real-world conditions, compared to idealized models.

Quantitative comparisons of several non-dominated solutions for mono-articular and bi-articular exoskeletons under both loading conditions, along with a detailed discussion, are presented in [71]. These comparisons indicate that although mono-articular and bi-articular exoskeletons achieve similar performance in the objective space, their distinct torque and power profiles lead to significantly different muscle coordination patterns. Notably, dominant muscles, such as the rectus femoris and psoas, exhibit varying activation. Bi-articular exoskeletons demonstrate more consistent torque and power profiles across loading conditions, making their response more predictable than mono-articular configurations.

Overall, these differences indicate that although both configurations can achieve comparable metabolic cost reductions, the mono-articular designs are more sensitive to loading, resulting in higher variability in torque delivery. This variability may complicate the design of control strategies, whereas the more predictable behavior of bi-articular exoskeletons could simplify controller development and enhance performance.

B. Inclusion of Inertial Effects on the Pareto Solutions

One of the key challenges in mobile exoskeleton design is minimizing mass/inertia, as they significantly increase metabolic power consumption during walking [58], [72], [73].

In our study, the bi-articular and mono-articular exoskeleton configurations exhibit distinct inertial properties due to differences in their kinematics, actuation, and peak torque requirements. Since OpenSim cannot simulate inertial variations beyond those captured during experimental data collection [28], we incorporate the detrimental inertial effects using the experimental metabolic model proposed by Browning et al. [58]. Their model, based on subjects walking at 1.25 m/s without load, closely matches the *noload* condition in our simulations [17], allowing us to superpose the additional metabolic cost due to exoskeleton mass/inertia onto our musculoskeletal simulation-based metabolic rate estimates.

Fig. 6 presents inertia-adjusted Pareto-fronts for both exoskeleton configurations, illustrating how inertial effects steepen the trade-off slope. With increased exoskeleton power consumption, the metabolic benefits diminish, since higher peak torques come at the cost of increased reflected inertia. Bi-articular exoskeletons perform better under inertial effects, as they introduce lower reflected inertia than mono-articular ones due to the more advantageous placement of the knee actuators. The performance degradation is greater for mono-articular devices with a median of 50.72% (interquartile range (IQR), 4.14) compared to bi-articular devices with a median of 38.67% (IQR, 4.88). Moreover, actuators with 70 Nm peak torque no longer remain as non-dominated solutions due to their high reflected inertia; under the inertial effects, non-dominated devices require a maximum of 60 Nm at the knee and 50 Nm at the hip joints, respectively.

These findings highlight the importance of actuator placement as well as promoting the utilization of high-torque density actuators to reduce reflected inertia and improve overall efficiency. Low transmission ratios enhance both actuation and regeneration efficiency, further benefiting exoskeleton performance. Additionally, placing actuators near proximal joints and transmitting power distally, such as using a parallelogram mechanism in the bi-articular designs, reduces reflected inertia. This principle mirrors human biomechanics, where bi-articular muscles minimize distal mass and transfer power efficiently, keeping a large portion of the muscle mass near the trunk.

Although bi-articular designs offer superior inertial properties, their mechanical implementation is more complex due to power transmission over a moving joint. A practical alternative is to modify mono-articular exoskeletons by relocating their knee actuator more proximally. Fig. D1 in *Supplementary Material* S5 studies different placements of the knee actuator: at the knee, on the upper thigh, and on the upper shank. Moving the actuator to the thigh improves performance by 9.50% (IQR, 0.47), while placing it on the shank offers a smaller improvement of 3.21% (IQR, 0.15). It is interesting to note that locating the actuator on the upper shank results in superior performance than placing it at the knee joint, as the metabolic cost of walking is less sensitive to inertia addition to the shank than inertia addition to the thigh [58].

This analysis underscores the critical role of inertial distribution in exoskeleton design, emphasizing the benefits of bi-articular actuation while presenting viable modifications for mono-articular configurations to mitigate inertial drawbacks. Furthermore, Fig. 6 provides a novel means for fair comparison of different exoskeleton designs and their corresponding optimal assistance torques under realistic inertial effects.

C. Selection Among the Non-Dominated Solutions

Once the Pareto-front solutions are computed for each exoskeleton configuration under different loading conditions and the inertial effects are superposed as depicted in Fig. 6, different exoskeletons can be rigorously compared to each other, allowing *an optimal* solution to be selected among all non-dominated solutions. The comparison in Fig. 6 indicates that, thanks to their favorable inertial properties, bi-articular exoskeleton configurations achieve superior metabolic cost

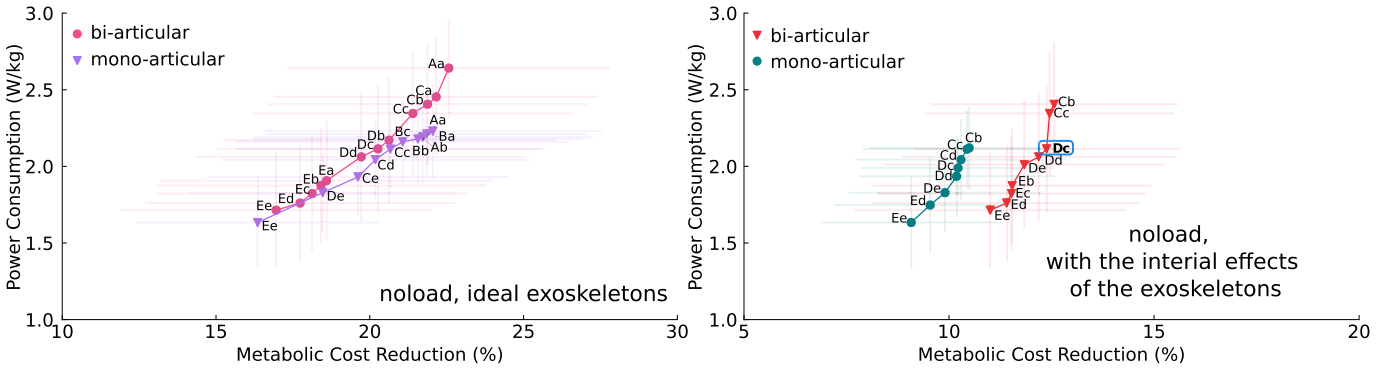

Fig. 6. Comparison of non-dominated solutions. The mono-articular and bi-articular exoskeleton configurations are compared under (a) ideal conditions, (b) considering the mass/inertia effects on metabolic power consumption. Higher torque capacities require larger transmission ratios; hence, significantly increase the reflected inertia and $I_{s,ratio}$. Accordingly, the metabolic cost increases due to inertial effects, and the inertia-adjusted Pareto front shifts left and exhibits a steeper trend relative to the cases with lower torque limits.

reductions compared to mono-articular devices, although some of them may incur higher power consumption.

On the other hand, one may consider that the implementation of bi-articular exoskeletons may be more challenging, and the inertial properties of mono-articular exoskeletons may be improved by a more favorable placement of the knee actuator unit, as illustrated in Fig. E1 of *Supplementary Material* S6. However, even with such favorable actuator placements for the mono-articular exoskeletons, bi-articular configurations still achieve higher metabolic cost reductions than those possible with the mono-articular exoskeletons. Along these lines, bi-articular exoskeletons provide a conclusively better choice in terms of metabolic cost reduction; hence, a design will be selected among them.

All solutions on the Pareto-front of bi-articular exoskeletons are optimal in the sense that no solution is unequivocally superior across all metrics; rather, each solution represents a different balance between metabolic efficiency and power use. A sample design selection can be made that provides a good balance between the competing factors for an intended application, and considering the primary design criteria, such as, the changes in muscle activities of the key lower limb muscles, the reaction forces/moments at the joints under assistance, and/or Modified Augmentation Factor (MAF), an extention of the Augmentation Factor (AF) proposed by Mooney et al. [2] that quantifies the normalized mechanical assistance provided to the user's center of mass during walking (see *Supplementary Material* S8 for the formal definition).

Inspecting the metabolic cost reduction and power consumption trade-off for bi-articular designs in Fig. 6, the non-dominated bi-articular exoskeleton configurations Cc and Cb are removed from the list of possible design selections, since they require excessive power consumption without providing significant improvements in metabolic cost reduction.

Among the designs shortlisted, the bi-articular exoskeleton Dc demonstrates a favorable balance, exhibiting a MAF value of 1.21 $\pm$ 0.67 W/kg under the *noload* walking condition. This value reflects a favorable trade-off between the magnitude of the assistance and the efficiency of the system. This value suggests that the exoskeleton provides sufficient mechanical support to meaningfully reduce muscular effort and metabolic cost while maintaining a reasonable actuator output relative to the user's body mass. Thus, the Dc configuration effectively promotes energy efficiency and biomechanically harmonious locomotion. Under the assistance torque profiles of the bi-articular exoskeleton Dc, systematic changes in muscle recruitment were observed, demonstrating reductions in energy-demanding muscles. (Please see *Supplementary Material* S7 for details.)

Based on these results, the bi-articular exoskeleton Dc, with 40 Nm peak torque at the hip and 50 Nm peak torque at the knee, is selected as the representative design. This configuration achieves a metabolic cost reduction of 20.26 $\pm$ 3.24% without accounting for inertial effects, and 12.38 $\pm$ 3.23% when inertial effects are considered, while maintaining a moderate power consumption of 2.11 $\pm$ 0.41 W/kg. The selected design is annotated in Fig. 6.

This selection highlights the importance of balancing metabolic benefits, power efficiency, and practical constraints, such as mass and inertia. Although the metabolic cost reduction drops when inertial effects are considered, the Dc configuration maintains a substantial assistance effect while avoiding excessive power demands. Its moderate actuator torque requirements simplify hardware implementation, and its favorable MAF value indicates effective assistance relative to the system's energy input. Overall, the bi-articular exoskeleton Dc represents a promising trade-off between performance, energy efficiency, and practicality for real-world prototyping.

Please note that the selection of an optimal exoskeleton design is application-dependent, and the bi-articular exoskeleton Dc is a sample choice among other valid ones. Overall, the designers may incorporate and prioritize various primary and secondary requirements for an intended application. Please refer to [71] for a comprehensive discussion of the design selection process and further insights into the underlying design trade-offs between mono- and bi-articular exoskeletons.

VI. Conclusion

This study introduced a systematic musculoskeletal simulation-based multi-criteria design optimization framework that enables rigorous comparisons among exoskeleton configurations and their assistance torque profiles by simultaneously optimizing metabolic cost reduction and power consumption. As another novel feature, our framework incorporates both the

negative effect of reflected inertia and the saturation of actuator torques on metabolic cost computations.

Incorporating realistic actuator torque limitations into our optimization framework reveals that sufficiently large torque limits minimally impact the assistance provided by both mono- and bi-articular exoskeleton configurations, while significantly reducing power consumption. When inertial effects are disregarded, both exoskeleton configurations achieve comparable performance levels, albeit with differing peak torque requirements; notably, mono-articular exoskeletons necessitate higher peak torque limits than their bi-articular counterparts. Pareto-front solutions under varying loading conditions demonstrate that actuator utilization and power consumption of bi-articular exoskeletons are less affected by subject loading compared to the mono-articular designs. Accordingly, bi-articular configurations exhibit more predictable responses to loading changes than those of mono-articular exoskeletons.

The inclusion of the detrimental effects of exoskeleton mass/inertia on the metabolic rates of walking indicates that bi-articular exoskeletons perform significantly better than mono-articular ones. Furthermore, the Pareto-optimal solutions for bi-articular configurations remain largely unchanged under the inertial effects, whereas mono-articular exoskeletons require a complete re-evaluation of non-dominated solutions.

Overall, the multi-criteria design optimization framework provides a basis for fair comparison among various exoskeletons and their optimal assistance torque profiles, considering actuator limits and the detrimental effects of reflected inertia on metabolic consumption. Hence, our design framework provides valuable *design guidelines* under realistic constraints, highlighting key trade-offs among metabolic cost reduction, power consumption, and inertial effects of exoskeletons.

Our musculoskeletal simulations have been validated against the literature [9], [17], as our framework recovers the ideal exoskeleton solutions as a special case. Given that all musculoskeletal simulation studies have certain limitations, the results of our study should be taken as guidelines and insights to inform the development of energy-efficient and effective exoskeletons for real-world applications. Please refer to *Supplementary Material* S9 for a detailed discussion of the validations and limitations of the study.

Acknowledgment

The work of Ali KhalilianMotamed Bonab was carried out during his graduate studies at Sabanci University.

References

[1] P. Malcolm, W. Derave, S. Galle, and D. De Clercq, "A simple exoskeleton that assists plantarflexion can reduce the metabolic cost of human walking," *PLoS ONE*, vol. 8, no. 2, Feb. 2013, Art. no. e56137.

[2] L. M. Mooney, E. J. Rouse, and H. M. Herr, "Autonomous exoskeleton reduces metabolic cost of human walking during load carriage," *J. NeuroEng. Rehabil.*, vol. 11, no. 1, pp. 1–11, Dec. 2014.

[3] S. H. Collins, M. B. Wiggin, and G. S. Sawicki, "Reducing the energy cost of human walking using an unpowered exoskeleton," *Nature*, vol. 522, no. 7555, pp. 212–215, Jun. 2015.

[4] G. Lee et al., "Reducing the metabolic cost of running with a tethered soft exosuit," *Sci. Robot.*, vol. 2, no. 6, pp. 31–6708, May 2017.

[5] D. E. Miller, G. R. Tan, E. M. Farina, A. L. Sheets-Singer, and S. H. Collins, "Characterizing the relationship between peak assistance torque and metabolic cost reduction during running with ankle exoskeletons," *J. NeuroEng. Rehabil.*, vol. 19, no. 1, p. 46, Dec. 2022.

[6] K. A. Witte, P. Fiers, A. L. Sheets-Singer, and S. H. Collins, "Improving the energy economy of human running with powered and unpowered ankle exoskeleton assistance," *Sci. Robot.*, vol. 5, no. 40, p. 9108, Mar. 2020.

[7] M. K. MacLean and D. P. Ferris, "Energetics of walking with a robotic knee exoskeleton," *J. Appl. Biomechanics*, vol. 35, no. 5, pp. 320–326, Oct. 2019.

[8] G. S. Sawicki, O. N. Beck, I. Kang, and A. J. Young, "The exoskeleton expansion: Improving walking and running economy," *J. NeuroEng. Rehabil.*, vol. 17, no. 1, pp. 1–9, Dec. 2020.

[9] T. K. Uchida, A. Seth, S. Pouya, C. L. Dembia, J. L. Hicks, and S. L. Delp, "Simulating ideal assistive devices to reduce the metabolic cost of running," *PLoS ONE*, vol. 11, no. 9, Sep. 2016, Art. no. e0163417.

[10] A. Seth et al., "OpenSim: Simulating musculoskeletal dynamics and neuromuscular control to study human and animal movement," *PLOS Comput. Biol.*, vol. 14, no. 7, Jul. 2018, Art. no. e1006223.

[11] J. C. Selinger, S. M. O'Connor, J. D. Wong, and J. M. Donelan, "Humans can continuously optimize energetic cost during walking," *Current Biol.*, vol. 25, no. 18, pp. 2452–2456, Sep. 2015.

[12] J. Kim et al., "Reducing the metabolic rate of walking and running with a versatile, portable exosuit," *Science*, vol. 365, no. 6454, pp. 668–672, Aug. 2019.

[13] D. F. N. Gordon, C. McGreavy, A. Christou, and S. Vijayakumar, "Human-in-the-loop optimization of exoskeleton assistance via online simulation of metabolic cost," *IEEE Trans. Robot.*, vol. 38, no. 3, pp. 1410–1429, Jun. 2022.

[14] J. P. Stingel, J. L. Hicks, S. D. Uhlrich, and S. L. Delp, "Simulating muscle-level energetic cost savings when humans run with a passive assistive device," *IEEE Robot. Autom. Lett.*, vol. 8, no. 10, pp. 6267–6274, Oct. 2023.

[15] E. P. Grabke, K. Masani, and J. Andrysek, "Lower limb assistive device design optimization using musculoskeletal modeling: A review," *J. Med. Devices*, vol. 13, no. 4, Dec. 2019, Art. no. 040801.

[16] S. H. L. Smith, R. J. Coppack, A. J. van den Bogert, A. N. Bennett, and A. M. J. Bull, "Review of musculoskeletal modelling in a clinical setting: Current use in rehabilitation design, surgical decision making and healthcare interventions," *Clin. Biomechanics*, vol. 83, Mar. 2021, Art. no. 105292.

[17] C. L. Dembia, A. Silder, T. K. Uchida, J. L. Hicks, and S. L. Delp, "Simulating ideal assistive devices to reduce the metabolic cost of walking with heavy loads," *PLoS ONE*, vol. 12, no. 7, Jul. 2017, Art. no. e0180320.

[18] D. J. Farris, J. L. Hicks, S. L. Delp, and G. S. Sawicki, "Musculoskeletal modelling deconstructs the paradoxical effects of elastic ankle exoskeletons on plantar-flexor mechanics and energetics during hopping," *J. Experim. Biol.*, vol. 217, no. 22, pp. 4018–4028, Nov. 2014.

[19] G. S. Sawicki and N. S. Khan, "A simple model to estimate plantarflexor muscle-tendon mechanics and energetics during walking with elastic ankle exoskeletons," *IEEE Trans. Biomed. Eng.*, vol. 63, no. 5, pp. 914–923, May 2016.

[20] B. Lim, S. Hyoung, J. Lee, K. Seo, J. Jang, and Y. Shim, "Simulating gait assistance of a hip exoskeleton: Case studies for ankle pathologies," in *Proc. IEEE Int. Conf. Robot. Autom.*, Sep. 2017, pp. 1022–1027.

[21] A. A. Nikooyan and A. A. Zadpoor, "Mass-spring-damper modelling of the human body to study running and hopping—An overview," *Proc. Inst. Mech. Eng., H, J. Eng. Med.*, vol. 225, no. 12, pp. 1121–1135, Dec. 2011.

[22] H. Aftabi, R. Nasiri, and M. N. Ahmadabadi, "Simulation-based biomechanical assessment of unpowered exoskeletons for running," *Sci. Rep.*, vol. 11, no. 1, pp. 1–12, Jun. 2021.

[23] A. K. Bonab, D. Leonardis, A. Frisoli, and D. Chiaradia, "Modeling, optimization, and musculoskeletal simulation of elbow-wrist exosuit," in *Proc. 21st Int. Conf. Adv. Robot. (ICAR)*, Dec. 2023, pp. 460–466.

[24] V. Q. Nguyen, B. R. Umberger, and F. C. Sup, "Predictive simulation of human walking augmented by a powered ankle exoskeleton," in *Proc. IEEE 16th Int. Conf. Rehabil. Robot. (ICORR)*, Jun. 2019, pp. 53–58.

[25] N. A. Bianco, P. W. Franks, J. L. Hicks, and S. L. Delp, "Coupled exoskeleton assistance simplifies control and maintains metabolic benefits: A simulation study," *PLoS ONE*, vol. 17, no. 1, Jan. 2022, Art. no. e0261318.

[26] M. L. Handford and M. Srinivasan, "Energy-optimal human walking with feedback-controlled robotic prostheses: A computational study," *IEEE Trans. Neural Syst. Rehabil. Eng.*, vol. 26, no. 9, pp. 1773–1782, Sep. 2018.

[27] S. L. Delp et al., "OpenSim: Open-source software to create and analyze dynamic simulations of movement," *IEEE Trans. Biomed. Eng.*, vol. 54, no. 11, pp. 1940–1950, Nov. 2007.

[28] J. L. Hicks, T. K. Uchida, A. Seth, A. Rajagopal, and S. L. Delp, "Is my model good enough? Best practices for verification and validation of musculoskeletal models and simulations of movement," *J. Biomechanical Eng.*, vol. 137, no. 2, Feb. 2015, Art. no. 020905.

[29] B. Ostraich and R. Riemer, "Rethinking exoskeleton simulation-based design: The effect of using different cost functions," *IEEE Trans. Neural Syst. Rehabil. Eng.*, vol. 32, pp. 2153–2164, 2024.

[30] Q. Meng, B. Kong, Q. Zeng, C. Fei, and H. Yu, "Concept design of hybrid-actuated lower limb exoskeleton to reduce the metabolic cost of walking with heavy loads," *PLoS ONE*, vol. 18, no. 5, May 2023, Art. no. e0282800.

[31] A. K. Bonab, D. Chiaradia, A. Frisoli, and D. Leonardis, "A framework for modeling, optimization, and musculoskeletal simulation of an Elbow–Wrist exosuit," *Robotics*, vol. 13, no. 4, p. 60, Apr. 2024.

[32] A. Rajagopal, C. L. Dembia, M. S. DeMers, D. D. Delp, J. L. Hicks, and S. L. Delp, "Full-body musculoskeletal model for muscle-driven simulation of human gait," *IEEE Trans. Biomed. Eng.*, vol. 63, no. 10, pp. 2068–2079, Oct. 2016.

[33] V. Firouzi, A. Davoodi, F. Bahrami, and M. A. Sharbafi, "From a biological template model to gait assistance with an exosuit," *Bioinspiration Biomimetics*, vol. 16, no. 6, Nov. 2021, Art. no. 066024.

[34] K. Junius, M. Moltedo, P. Cherelle, C. Rodriguez-Guerrero, B. Vanderborght, and D. Lefeber, "Biarticular elements as a contributor to energy efficiency: Biomechanical review and application in bio-inspired robotics," *Bioinspiration Biomimetics*, vol. 12, no. 6, Nov. 2017, Art. no. 061001.

[35] B. I. Prilutsky, L. N. Petrova, and L. M. Raitsin, "Comparison of mechanical energy expenditure of joint moments and muscle forces during human locomotion," *J. Biomechanics*, vol. 29, no. 4, pp. 405–415, Apr. 1996.

[36] R. P. Wells, "Mechanical energy costs of human movement: An approach to evaluating the transfer possibilities of two-joint muscles," *J. Biomechanics*, vol. 21, no. 11, pp. 955–964, Jan. 1988.

[37] D. G. Thelen, F. C. Anderson, and S. L. Delp, "Generating dynamic simulations of movement using computed muscle control," *J. Biomechanics*, vol. 36, no. 3, pp. 321–328, Mar. 2003.

[38] B. R. Umberger, K. G. M. Gerritsen, and P. E. Martin, "A model of human muscle energy expenditure," *Comput. Methods Biomechanics Biomed. Eng.*, vol. 6, no. 2, pp. 99–111, May 2003.

[39] T. K. Uchida, J. L. Hicks, C. L. Dembia, and S. L. Delp, "Stretching your energetic budget: How tendon compliance affects the metabolic cost of running," *PLoS ONE*, vol. 11, no. 3, Mar. 2016, Art. no. e0150378.

[40] P. Y. Papalambros and D. J. Wilde, *Principles of Optimal Design: Modeling and Computation*. Cambridge, U.K.: Cambridge Univ. Press, 2000.

[41] R. Unal, G. Kiziltas, and V. Patoglu, "A multi-criteria design optimization framework for haptic interfaces," in *Proc. Symp. Haptic Interface Virtual Environ. Teleoperator Syst.*, Mar. 2008, pp. 231–238.

[42] R. T. Marler and J. S. Arora, "The weighted sum method for multi-objective optimization: New insights," *Struct. Multidisciplinary Optim.*, vol. 41, no. 6, pp. 853–862, Jun. 2010.

[43] R. Unal, G. Kiziltas, and V. Patoglu, "Multi-criteria design optimization of parallel robots," in *Proc. IEEE Conf. Robot., Autom. Mechatronics*, Sep. 2008, pp. 112–118.

[44] Y. Aydin, O. Tokatli, V. Patoglu, and C. Basdogan, "A computational multicriteria optimization approach to controller design for physical human–robot interaction," *IEEE Trans. Robot.*, vol. 36, no. 6, pp. 1791–1804, Dec. 2020.

[45] A. Kamadan, G. Kiziltas, and V. Patoglu, "Co-design strategies for optimal variable stiffness actuation," *IEEE/ASME Trans. Mechatronics*, vol. 22, no. 6, pp. 2768–2779, Dec. 2017.

[46] J. Merlet, *Parallel Robots*. Dordrecht, The Netherlands: Springer, 2006.

[47] U. Mengilli, Z. O. Orhan, U. Caliskan, and V. Patoglu, "Passivity of series damped elastic actuation under velocity-sourced impedance control," in *Proc. IEEE World Haptics Conf. (WHC)*, Jul. 2021, pp. 379–384.

[48] C. U. Kenanoglu and V. Patoglu, "Passive realizations of series elastic actuation: Effects of plant and controller dynamics on haptic rendering performance," *IEEE Trans. Haptics*, vol. 17, no. 4, pp. 882–899, Oct. 2024.

[49] O. T. Kenanoglu, C. U. Kenanoglu, and V. Patoglu, "Effect of low-pass filtering on passivity and rendering performance of series elastic actuation," *IEEE Trans. Haptics*, vol. 16, no. 4, pp. 567–573, Oct. 2023.

[50] C. U. Kenanoglu and V. Patoglu, "Effect of inherent damping of the series elastic element on rendering performance and passivity of interaction control," *J. Dyn. Syst., Meas., Control*, vol. 147, no. 5, Sep. 2025, Art. no. 051008.

[51] F. E. Tosun and V. Patoglu, "Necessary and sufficient conditions for the passivity of impedance rendering with velocity-sourced series elastic actuation," *IEEE Trans. Robot.*, vol. 36, no. 3, pp. 757–772, Jun. 2020.

[52] C. U. Kenanoglu and V. Patoglu, "Effect of reduced-order modelling on passivity and rendering performance analysis of series elastic actuation," *IEEE Robot. Autom. Lett.*, vol. 10, no. 6, pp. 5745–5752, Jun. 2025.

[53] M. A. Ergin and V. Patoglu, "A self-adjusting knee exoskeleton for robot-assisted treatment of knee injuries," in *Proc. IEEE/RSJ Int. Conf. Intell. Robots Syst.*, Sep. 2011, pp. 4917–4922.

[54] M. Yalcin and V. Patoglu, "Kinematics and design of AssistOn-SE: A self-adjusting shoulder-elbow exoskeleton," in *Proc. 4th IEEE RAS EMBS Int. Conf. Biomed. Robot. Biomechatronics (BioRob)*, Jun. 2012, pp. 1579–1585.

[55] M. A. Ergin and V. Patoglu, "ASSISTON-SE: A self-aligning shoulder-elbow exoskeleton," in *Proc. IEEE Int. Conf. Robot. Autom.*, May 2012, pp. 2479–2485.

[56] B. Celebi, M. Yalcin, and V. Patoglu, "AssistOn-knee: A self-aligning knee exoskeleton," in *Proc. IEEE/RSJ Int. Conf. Intell. Robots Syst.*, Nov. 2013, pp. 996–1002.

[57] A. Erdogan, B. Celebi, A. C. Satici, and V. Patoglu, "Assist on-ankle: A reconfigurable ankle exoskeleton with series-elastic actuation," *Auto. Robots*, vol. 41, no. 3, pp. 743–758, Mar. 2017.

[58] R. C. Browning, J. R. Modica, R. Kram, and A. Goswami, "The effects of adding mass to the legs on the energetics and biomechanics of walking," *Med. Sci. Sports Exerc.*, vol. 39, no. 3, pp. 515–525, 2007.

[59] R. T. Marler and J. S. Arora, "Survey of multi-objective optimization methods for engineering," *Struct. Multidisciplinary Optim.*, vol. 26, no. 6, pp. 369–395, Apr. 2004.

[60] K. Miettinen, F. Ruiz, and A. P. Wierzbicki, *Introduction to Multiobjective Optimization: Interactive Approaches*. Berlin, Germany: Springer, 2008, pp. 27–57.

[61] W. Jakob and C. Blume, "Pareto optimization or cascaded weighted sum: A comparison of concepts," *Algorithms*, vol. 7, no. 1, pp. 166–185, Mar. 2014.

[62] Y. Haimes, "On a bicriterion formulation of the problems of integrated system identification and system optimization," *IEEE Trans. Syst., Man, Cybern.*, vol. SMC-1, no. 3, pp. 296–297, Mar. 1971.

[63] M. Laumanns, L. Thiele, and E. Zitzler, "An efficient, adaptive parameter variation scheme for metaheuristics based on the epsilon-constraint method," *Eur. J. Oper. Res.*, vol. 169, no. 3, pp. 932–942, Mar. 2006.

[64] K. Chircop and D. Zammit-Mangion, "On-constraint based methods for the generation of Pareto frontiers," *J. Mech. Eng. Autom.*, vol. 3, no. 5, pp. 279–289, 2013.

[65] B. Penzlin, L. Bergmann, Y. Li, L. Ji, S. Leonhardt, and C. Ngo, "Design and first operation of an active lower limb exoskeleton with parallel elastic actuation," *Actuat.*, vol. 10, no. 4, p. 75, 2021.

[66] S. Yu et al., "Design and control of a high-torque and highly backdrivable hybrid soft exoskeleton for knee injury prevention during squatting," *IEEE Robot. Autom. Lett.*, vol. 4, no. 4, pp. 4579–4586, Oct. 2019.

[67] K. A. Witte, A. M. Fatschel, and S. H. Collins, "Design of a lightweight, tethered, torque-controlled knee exoskeleton," in *Proc. Int. Conf. Rehabil. Robot. (ICORR)*, Jul. 2017, pp. 1646–1653.

[68] T. Vouga, J. Fasola, R. Baud, A. R. Manzoori, J. Pache, and M. Bouri, "TWIICE one powered exoskeleton: Effect of design improvements on usability in daily life as measured by the performance in the CYBATHLON race," *J. NeuroEng. Rehabil.*, vol. 19, no. 1, p. 63, Dec. 2022.

[69] P. de Leva, "Adjustments to Zatsiorsky–Seluyanov's segment inertia parameters," *J. Biomechanics*, vol. 29, no. 9, pp. 1223–1230, Sep. 1996.

[70] IBM Corp.(2017). *IBM SPSS Statistics for Windows*. [Online]. Available: https://www.ibm.com/analytics/spss-statistics-software

[71] A. K. Bonab, "Simulation-based optimal design of exoskeletons to reduce metabolic cost and improve energy efficiency," M.S. thesis, Mechtron. Eng., Sabanci Univ., Istanbul, Turkiye, 2021.

[72] T. D. Royer and P. E. Martin, "Manipulations of leg mass and moment of inertia: Effects on energy cost of walking," *Med. Sci. Sports Exercise*, vol. 37, no. 4, pp. 649–656, Apr. 2005.

[73] R. G. Soule and R. F. Goldman, "Energy cost of loads carried on the head, hands, or feet," *J. Appl. Physiol.*, vol. 27, no. 5, pp. 687–690, Nov. 1969.